Document ID:
Revision ID: 0
Effective Date: 09/17/2020
INL/EXT-20-59704

Report

Project No. 33486

Neutron Absorber Material Corrosion Testing Preliminary Report

Tedd E. Lister
Ronald E. Mizia
Luis A. Diaz
Michael G. Jones

The INL is a U.S. Department of Energy National Laboratory operated by Battelle Energy Alliance.

Idaho National Laboratory

Neutron Absorber Material Corrosion Testing Report	Identifier:		
	Revision:	0	
	Effective Date:	09/17/2020	Page: 1 of 22

Prepared by:

Tedd E. Lister	09/17/2020
	Date

Approved by:

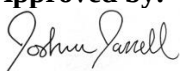

Joshua Jarrell	09/17/2020
	Date

REVISION LOG

Rev.	Date	Affected Pages	Revision Description
0	09/17/2020	All	Initial issue

Acronyms

ASTM	ASTM International
ACS	American Chemical Society
ANA	Advanced Neuron Absorbing Alloy
BB	Bohler Bleche
BSS	Borated stainless steel
CarTech	Carpenter Technology Corporation
CPP	Cyclic potential polarization
CSNF	Commercial spent nuclear fuel
E_{corr}	Corrosion potential
E_{pit}	Pitting potential
E_{rp}	Repassivation potential
HVAF	High velocity air fuel
HVOF	High velocity oxygen fuel
INL	Idaho National Laboratory
LLC	Limited liability company
LLNL	Lawrence Livermore National Laboratory
LPR	Linear polarization resistance
NAM	Neutron absorbing material
NSNFP	National Spent Nuclear Fuel Program
ORNL	Oak Ridge National Laboratory
RO	Reverse osmosis
SNL	Sandia National Laboratory
SAM	Structurally Amorphous Materials
SS	Stainless steel
YMP	Yucca Mountain Project

1. Introduction

Neutron absorbing materials (NAMs) are used within commercial spent nuclear fuel (CSNF or commercial SNF) canisters to maintain nuclear subcriticality in the unlikely circumstance that a canister is breached during storage or transportation and then is flooded with water, which is a neutron moderator. Including NAMs within CSNF canisters absorbs neutrons and thereby reduces the potential for criticality events. For the 2020 fiscal year, INL has been tasked to revive the testing portion of a neutron absorber development program supported by the National Spent Nuclear Fuel Program (NSNFP) and later by the Yucca Mountain Project (YMP). Previous work focused on two classes of materials: commercially produced borated stainless steels (BSS) and INL developed nickel-based alloys with gadolinium added as a neutron absorber. This report will provide initial results from corrosion testing performed during the 2020 fiscal year. These results are incomplete, as specimen analysis as of the time of writing are an ongoing activity. The testing was performed according to INL PLN-6095, which was formulated though consensus with staff at Oak Ridge National Laboratory (ORNL), Sandia National Laboratory (SNL) and INL [1].

2. Experimental

Testing was performed using ASTM G5 as a guide [2]. Experiments were performed to step-by-step procedures with checklists to ensure consistency. The checklists are companions to the laboratory notebooks which fully documents the testing. The two testing stations used are separately identified and tests were staggered to avoid specimens being switched, as specimen ID markings were not employed.

2.1 Specimens

The following alloy types were tested: Type 304L stainless steel (SS), Type 316L SS, 304B4 SS, 304B5 SS, Alloy 22, M326 (low Cr) Advanced Neutron Absorber (ANA) and M327 (high Cr) ANA. The composition of the materials are shown in Table 1 below, obtained from heat papers or through analysis performed by previous testing programs. Type 304L and 316L SS were obtained from Metal Samples finished to 600 grit SiC. Alloy 22 specimens were obtained from Metal Samples. ANA (also called Ni-Cr-Mo-Gd) specimens were remaining materials either machined by Metal Samples or INL machine shop with 600 grit SiC finish. BSS were remaining specimens from previous testing activities.

Table 1. Composition of alloys used in this testing.

Material	ANA	ANA	Alloy 22	304B4	304B5	304L	316L
Heat	M326	M327	2277-7-3130	182194	182195		AZ608
Molybdenum	14.53	14.32	13.47			0.33	2.018
Chromium	14.71	21.01	21.55	19.46	19.36	18.27	16.57
Gadolinium	2	1.98					
Boron				1.17	1.32		
Oxygen	0.0032	0.0042					
Nitrogen						0.069	0.034
Phosphorus			0.007			0.022	0.03
Manganese	0.001	0.01	0.25	1.91	1.84	1.64	
Magnesium	0.002	0.002					
Nickel	Bal	Bal	Bal	13.39	13.39	8.41	10.5
Iron	0.025	0.032	3.54	Bal	Bal	Bal	Bal
Cobalt	0.009	0.003	0.74			0.12	0.21
Carbon	0.006	0.001	0.003	0.05	0.05	0.02	0.022
Silicon	0.013	0.018	0.024			0.44	0.27
Sulfur	0.001	0.002	0.004			0.024	0.0215
Copper						0.35	0.31
Vanadium			0.12				
Tungsten			2.83				

The specimens were of the boldly exposed type (no intentionally designed crevices) which were cylinders approximately 1.7” length and 0.25” diameter attached to a threaded rod. The rod was isolated from solution contact by a glass tube with a flat Viton gasket sealing the submerged interface. For 304B4 and 304B5, crevice specimens were employed as they were the only available specimens. The specimens were 0.75” x 0.75” x 0.375” blocks with a 0.325” through hole machined into the larger area surfaces. These specimens were tested without crevice assemblies. Teflon gaskets were used to seal between the glass and specimen. The 304B5 specimens were refinished test specimens from previous work as no untested specimens exist. Specimens were cleaned by a sequential rinse in acetone, ethanol and deionized water to remove grease and other detritus prior to testing. The specimens were weighed on a 5-place balance before and after testing.

2.2 Solution preparation

Three solutions have been included in this work: artificial seawater, 0.028 M NaCl and 0.1 M HCl. Solutions were made using American Chemical Society (ACS) grade chemicals. A calibrated three-place balance was used to weigh chemicals. These weights were recorded in laboratory notebooks and/or data

sheets. Water was be obtained from the reverse osmosis (RO) purification system, which is fed by a building RO water system. The final water conductivity was 18 MΩ–cm. The solution volume for the tests was 900 mL. ASTM D1141 was used as a guide to produce artificial seawater [3].

2.3 Electrochemical cell

The electrochemical cell was based on ASTM G5 specification [2]. The cell and associated accessories were made of borosilicate glass. The cell has facilities for gas purging through a ceramic frit (150 cm^3/min). A glass condenser, through which gas exited the cell, was employed to reduce water evaporation during the test. All tests were performed at 30 ºC. Temperature was set through a thermocouple-controlled heating mantle. Thermocouples were checked for tolerance at INL calibration labs. A graphite rod was used as the counter electrode, cleaned and or replaced regularly. Commercially sourced (Pine Instruments) reference electrodes, of the Ag/AgCl (4 M KCl) type (0.199 V vs. normal hydrogen electrode), were compared to two reference electrodes (of the same type and source) set aside specifically as standards.

2.4 Electrochemical testing sequence:

Electrochemical testing was performed using a prescribed sequence that 1) measures the corrosion potential (E_{corr}) with air purge, 2) measures the E_{corr} with N_2 purge while removing oxygen from step 1, 3) performs three linear polarization resistance (LPR) tests, and 4) performs a cyclic potential polarization (CPP) test from 0.2 V negative of the measured E_{corr} in N_2. LPR tests were performed by stepping from E_{corr} to -30 mV negative and sweeping positive 60 mV (sweep of ±30 mV of E_{corr}). ASTM G59 was used as a basis for designing the tests [4]. For CPP, the anodic switching potential varied with specimen type, where SSs displayed excessive pitting if swept too far positive in comparison to nickel-based alloys. The scan rate for LPR and CPP was 0.6 V/hr (0.167 mV/sec).

2.5 Post-test analysis

Data was analyzed using software included with the potentiostat. Specific calculations for corrosion rates were based on guidelines obtained from ASTM G102 [5]. The corrosion rate was calculated using EC-Lab software (Version 11.34) provided with the BioLogic potentiostat. For CPP curve analysis, the final E_{corr} in air provides a value of where the alloy potential resides in equilibrium with air. The pitting potential (E_{pit}) was estimated as the potential where the potentially rapidly increases, The repassivation potential (E_{rp}) was estimated as the value where the reverse sweep crossed zero current (switched from positive to negative). For SS specimens, this was not always observed and the E_{rp} was deemed to be where a sharp deviation in the current drop on the return sweep occurred. Specimens were weighed before

and after testing with the difference reported. No attempts were made to descale specimens and visually significant scaling was not observed.

2.6 Specimen and solution analysis

Specimen analysis is ongoing as of the time this report was issued. Several methods are being employed: photography, optical microscopy, and scanning electron microscopy. Measurement of pit depths may be performed using and optical microscope with a z-calibrated motor. In the future, specimens will be available to perform other analysis methods as deemed useful to interpretation of results. A volume of test solution has been captured and will be kept for possible future analysis, which will be performed when deemed useful to interpretation of results.

3. Results

3.1 Corrosion testing results

3.1.1 E_{corr} test results

The corrosion potential of specimens in solutions purged with air (E_{corr}) was measured for 4 hours and the last value was recorded. In the event of transient response at the end of the measurement, a point prior to the final point was selected that is more representative of the E_{corr}. This value places the equilibrium potential in an air saturated solution. Data for E_{corr} determined from the curves is presented with the CPP data in Table 3. The E_{corr} curves for SS in seawater are shown in Figure 1. Both 304L and 304B4 show several negative going transients which are indicative of localized corrosion [6] while the 316L specimen is mostly smooth. This agrees with known performance differences of 304L and 316L, where the Mo containing 316 is often selected over 304 for marine service [7]. The curve for 304B5 shows some transient activity earlier, but a smooth curve afterwards.

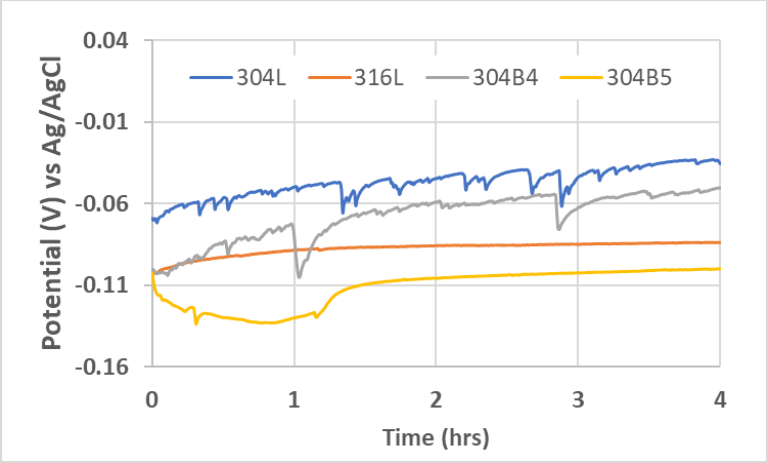

Figure 1. E_{corr} traces for SS alloys in seawater.

Figure 2 shows E_{corr} curves for nickel-based alloys. Alloy 22 has a smooth curve while the ANA specimens both show transient responses indicative of localized corrosion. Previous work has identified the secondary phase as possessing poor corrosion characteristics [8]. The Ni_5Gd secondary phase selectively dissolves as it has little Cr and thus does not form an effective passive film.

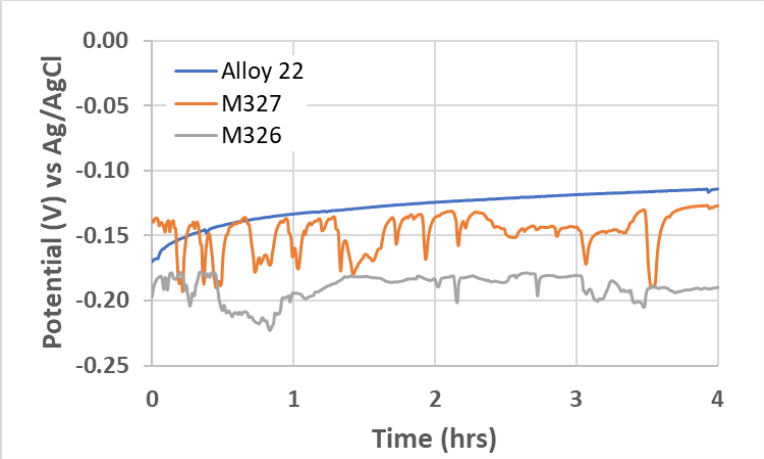

Figure 2. E_{corr} traces for nickel-based alloys in seawater.

3.1.2 LPR test results

After measuring E_{corr} with N_2 purge, three LPR sweeps were performed to measure the general corrosion rate. Table 2 shows the average corrosion rates obtained in testing. In cases were LPR data was not recorded, it is thought that localized corrosion interfered with the current data. In these tests, measured E_{corr} values had signatures of pitting corrosion, where negative drops in potential during pitting and metastable pitting events [6]. Specimens generally demonstrate low corrosion rates for 0.028 M NaCl and seawater, while several orders of magnitude higher for 0.1 M HCl. Alloy 22 being the exception, showing low corrosion rates in 0.1 M HCl.

Table 2. General corrosion rate data from LPR.

Date	Alloy	Solution	Rate (mmpy)
7/27/2020	Alloy 22	0.028 M NaCl	7.94E-06
8/6/2020	M327	0.028 M NaCl	1.15E-04
8/19/2020	M327	0.028 M NaCl	4.74E-05
8/11/2020	M326	0.028 M NaCl	-
8/17/2020	M326	0.028 M NaCl	9.64E-04
8/21/2020	M326	0.028 M NaCl	1.25E-05
7/29/2020	316L	0.028 M NaCl	9.20E-05
8/3/2020	304L	0.028M NaCl	-
8/26/2020	304B4	0.028 M NaCl	1.22E-05
9/4/2020	304B4	0.028 M NaCl	1.74E-04
9/8/2020	304B5	0.028 M NaCl	-
7/28/2020	Alloy 22	seawater	4.19E-06
8/7/2020	M327	seawater	-
8/25/2020	M327	seawater	-
8/26/2020	M327	seawater	4.66E-05
8/12/2020	M326	seawater	6.93E-06
8/20/2020	M326	seawater	1.87E-05
7/30/2020	316L	seawater	2.38E-06
9/2/2020	316L	seawater	9.20E-06
8/4/2020	304L	seawater	-
9/15/2020	304L	seawater	6.91E-06
9/3/2020	304B4	seawater	1.14E-05
9/9/2020	304B5	seawater	2.58E-04
7/29/2020	Alloy 22	0.1 M HCl	2.02E-05
8/10/2020	M327	0.1M HCl	1.15E-01
8/21/2020	M327	0.1M HCl	1.42E-02
8/13/2020	M326	0.1M HCl	-
8/18/2020	M326	0.1M HCl	4.33E-01
8/27/2020	M326	0.1M HCl	5.57E-02
7/30/2020	316L	0.1 M HCl	2.19E-02
8/5/2020	304L	0.1 M HCl	1.41E-04
8/27/2020	304B4	0.1M HCl	6.81E-02
9/10/2020	304B5	0.1M HCl	4.72E-02

mmpy: millimeters per year

3.1.3 CPP test results

CPP tests were performed following LPR tests. These tests provide understanding of the specimen corrosion and electrochemical characteristics in the environments as a function of potential. Two important parameters are obtained from the curves, the E_{pit} and E_{rp}. E_{pit} is defined as the point where a

sharp increase in current is observed in the forward sweep. It can be thought of as the initiation point for pitting corrosion. E_{rp} is defined as the point at where the current from pitting has subsided, typically the point at which current switches sign (net reducing current flowing). This would indicate the point where the material is defined as stable. E_{corr} is typically compared to E_{rp} to assess stability to pitting corrosion, where the more positive E_{rp} is relative to E_{corr}, the less likely pitting corrosion will occur. Conversely, if the E_{corr} is more positive than E_{rp}, the alloy and environment are generally not compatible. This section will feature curves obtained in seawater as the initial analysis performed with other solutions to follow.

CPP curves for 304L and 316L are shown in Figure 3. The forward curve (positive scan direction) starts negative of the measured E_{corr} value and for both alloys displays a response typical of chloride containing solutions, where on the forward sweep small transients are observed approaching E_{pit}, followed by a rapid growth in current. The E_{pit} is significantly more positive for 316L. On the return sweep the current is sustained such that the current exceeds (hysteresis) that of the forward sweep. The increased current is due to active pit dissolution. This positive (anodic) current eventually declines as oxide film reform on the surface of the formed pits. The point at which this occurs is defined as the E_{rp}. Note that for 316L, there was not a change in sign, so the E_{rp} was chosen where the current stabilized on the return sweep. While 316L displayed a drop in current more positive than 304L, the actual E_{rp} values were not significantly different, showing the value of comparing curves versus relying on specific values.

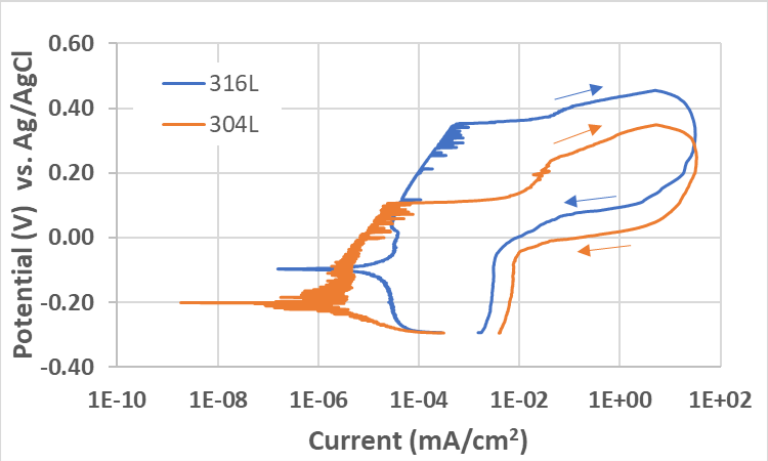

Figure 3. CPP curves for SS Type 304L and Type 316L.

Figure 4 shows CPP plots for the two BSS specimens in seawater. In the forward sweep, the 304B5 shows a higher E_{pit} value despite having a higher B content (1.17 vs. 1.32 wt.%). This was observed when comparing these two alloys (same heat) in dilute chloride/sulfate/nitrate containing solutions previously

[9]. On the return sweep, a significant hysteresis is observed for both specimens with E_{rp} value very similar to those observed for 304L and 316L specimens, with 304B5 being only slightly more negative. Again, the current did not change signs, similar to what was observed in Figure 3.

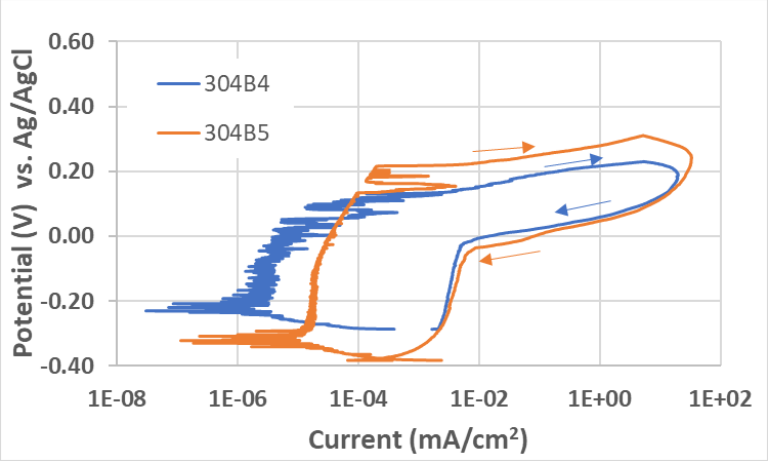

Figure 4. CPP curves for 304B4 and 304B5 alloys.

The curve for Alloy 22 is presented in Figure 5. The Alloy 22 specimen showed low current and no evidence of pitting corrosion due to the lack of hysteresis in the return sweep. Alloy 22 possesses well-known stability in high chloride environments, where it is considered “practically immune to pitting corrosion” [10].

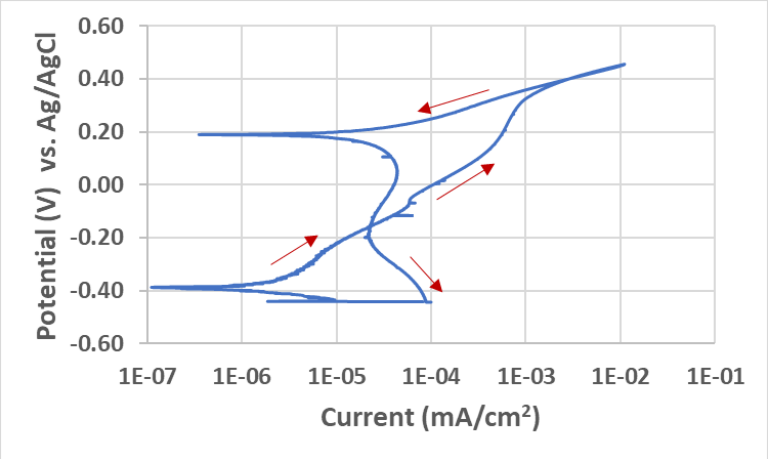

Figure 5. CPP curves for Alloy 22 in seawater.

Curves for the two ANA specimens are shown in Figure 6. In comparison to Alloy 22, both ANA specimens show significantly greater current in the passive region. On the return sweeps, there is not a

typical hysteresis from corrosion pits growth such as observed for SSs. For higher Cr M327 alloy, there is lower overall current, although there is a slightly greater current in the return sweep compared to the forward sweep. For the M326 alloy a greater current was observed, however the return sweep shows lower current than the forward sweep. Due to the secondary phase, the pitting corrosion of these alloys is more complex. The prevailing (but untested) thought is that corrosion decreases after the secondary phase is dissolved.

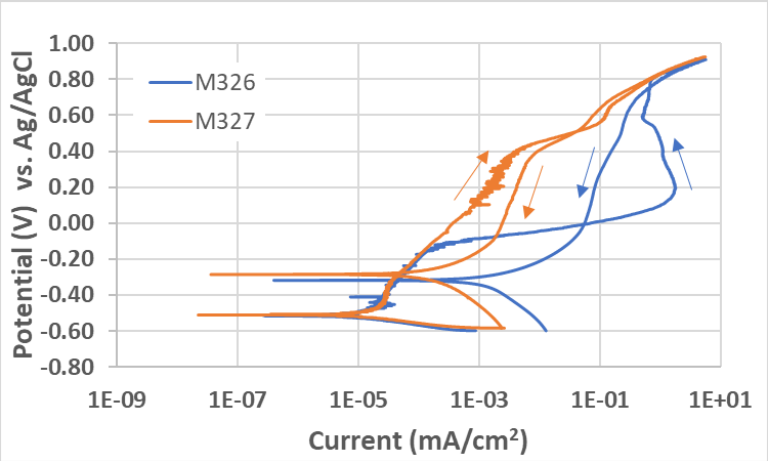

Figure 6. CPP curves for ANA alloys M326 and M327 in seawater.

An initial assessment of the CPP curves for all three solutions was performed as reported in Table 3. In some cases, the CPP curves do not allow a definitive value to be reported. Alloy 22 did not show signs of pitting corrosion, which agrees with previous work [ref 10 as example]. The reported E_{rp} values for Alloy 22 are where the current changes sign, far positive of any other alloy. For SS specimens, E_{rp} was not clearly defined, as current generally did not cross zero. The values presented are based on where current reaches a transition from decreasing to stabilizing at a low positive value. Consultation on how to treat this situation will be sought through literature and standards. In the assessment here, the E_{rp} was not clearly different for any of the SS alloys. However, E_{pit} for 316L was significantly higher than other SS alloys suggesting a lower probability to initiate corrosion. ANA specimens show peculiar CPP sweeps as detailed above. Based on previous work [8], surface damage to the specimens was limited to where secondary phase particles intersected the surface. Characteristics of the curves are based on to what level the secondary phase has been dissolved. As an example, for M327 in 0.1 M HCl, the curve on 8/21/2020 was scanned further positive than the one for 08/10/2020 and showed a more positive E_{rp}. Presumably, the more positive scan in a the most corrosive solution removed more of the secondary phase intersecting the

surface. A more positive E_{rp} indicates a more corrosion resistant material. Future work should explore specimens after acid pickling to remove the secondary phase.

Table 3. Corrosion parameters obtained from CPP tests.

Date	Alloy	Solution	E_{corr}	E_{rp}	E_{pit}	Hysteresis loop	E_{corr} notes
7/27/2020	Alloy 22	0.028 M NaCl	-0.0026	0.366	none	N	S
8/6/2020	M327	0.028 M NaCl	-0.0534	-0.343	-0.164	S	T
8/19/2020	M327	0.028 M NaCl	-0.135	-0.285	none	N	T
8/11/2020	M326	0.028 M NaCl	-0.0891	-0.335	-0.0349	S	T
8/17/2020	M326	0.028 M NaCl	-0.137	-0.324	none	N	T
8/21/2020	M326	0.028 M NaCl	-0.141	-0.273	none	N	T
7/29/2020	316L	0.028 M NaCl	0.0237	0.0828	0.339	L	S
8/3/2020	304L	0.028M NaCl	0.0223	-0.0938	0.267	L	T
8/26/2020	304B4	0.028 M NaCl	0.0163	0.0645	0.345	L	T
9/4/2020	304B4	0.028 M NaCl	0.0606	0.0544	0.216	L	T
9/8/2020	304B5	0.028 M NaCl	-0.0384	0.0189	0.365	L	T
7/28/2020	Alloy 22	seawater	-0.144	0.19	none	N	S
8/7/2020	M327	seawater	-0.127	-0.353	-0.0676	S	T
8/26/2020	M327	seawater	-0.291	-0.285	0.448	S	T
8/12/2020	M326	seawater	-0.174	-0.388	-0.153	S	T
8/20/2020	M326	seawater	-0.189	-0.317	none	N	T
7/30/2020	316L	seawater	-0.0837	-0.075	0.362	L	S
9/2/2020	316L	seawater	-0.0479	-0.0756	0.348	L	S
8/4/2020	304L	seawater	-0.033	-0.137	0.156	L	T
9/15/2020	304L	seawater	-0.0205	-0.0754	0.107	L	T
9/1/2020	304B4	seawater	-0.0142	-0.0236	0.207	L	T
9/3/2020	304B4	seawater	-0.0502	-0.0249	0.133	L	T
9/9/2020	304B5	seawater	-0.0998	-0.0862	0.214	L	T
7/29/2020	Alloy 22	0.1 M HCl	0.141	0.51	none	N	S
8/10/2020	M327	0.1M HCl	-0.273	-0.217	none	N	-
8/21/2020	M327	0.1M HCl	-0.226	-0.0392	none	N	S
8/18/2020	M326	0.1M HCl	-0.216	-0.244	none	N	S
8/27/2020	M326	0.1 M HCl	-0.227	-0.226	none	S	T
7/30/2020	316L	0.1 M HCl	-0.0179	-0.199	0.109	S	T
8/5/2020	304L	0.1 M HCl	-0.0191	-0.0642	0.116	L	T
8/27/2020	304B4	0.1 M HCl	-0.239	-0.0207	0.307	L	T
9/10/2020	304B5	0.1M HCl	-0.239	-0.3	0.0441	S	T

Hysteresis loop: none (N), small (S), large (L),
E_{corr}: smooth (S), transients (T)

3.1.4 Gravimetric results and post-test observations

Specimens were weighed and photographed before and after testing. Table 4 presents the weight change scaled to surface area as well as providing visual observations captured by photographs. For localized corrosion, which appears to be the prime weight loss route, weight change should not be considered proportional to corrosion rate. Note that the reversing potential for the forward sweep greatly influences the weight loss. The measurement can be used in some cases to assess test results. Given the quite different CPP curves, standardizing the switching potential does not make sense. Observations are based on photographs taken after testing.

Table 4. Gravimetric analysis and observations made after CPP tests.

Date	Alloy	Solution	Mass (g/cm^2)	Visual observations
7/27/2020	Alloy 22	0.028 M NaCl	0.00000	No clear change
8/6/2020	M327	0.028 M NaCl	-0.00001	No clear change
8/19/2020	M327	0.028 M NaCl	-0.00163	Dull with localized stains, no clear pits
8/11/2020	M326	0.028 M NaCl	-0.00198	Mostly shiny with isolated brown stains, no
8/17/2020	M326	0.028 M NaCl	-0.00150	Bright no clear pits observed
8/21/2020	M326	0.028 M NaCl	-0.00221	Dull, no pits
7/29/2020	316L	0.028 M NaCl	0.00000	No clear change
8/3/2020	304L	0.028M NaCl	-0.00001	No clear change
8/26/2020	304B4	0.028 M NaCl	-0.00111	Shiny with localized brown stains, hint of
9/4/2020	304B4	0.028 M NaCl	-0.00143	Shiny, widespread small pits
9/8/2020	304B5	0.028 M NaCl	-0.00153	Shiny, widespread small pits
7/28/2020	Alloy 22	seawater	-0.00055	No clear change
8/7/2020	M327	seawater	0.00001	No clear change
8/26/2020	M327	seawater	-0.00060	Dull, isolated small pits
8/12/2020	M326	seawater	-0.00236	Mostly shiny with isolated brown stains, no
8/20/2020	M326	seawater	-0.00235	Dull, small isolated pits
7/30/2020	316L	seawater	0.00032	Brown coloration, no pitting
9/2/2020	316L	seawater	-0.01136	Dull with widespread, long small pits
8/4/2020	304L	seawater	0.00000	Mostly shiny, no pitting
9/15/2020	304L	seawater	-0.01071	Shiny with brown stain, narrow deep pits
9/3/2020	304B4	seawater	-0.00317	Dull, widespread pitting
9/9/2020	304B5	seawater	-0.00769	Dull, widespread deep but small pits
7/29/2020	Alloy 22	0.1 M HCl	0.00000	No clear change
8/10/2020	M327	0.1M HCl	-0.00072	No clear change
8/21/2020	M327	0.1M HCl	-0.00029	Mostly shiny with localized brown stains,
8/13/2020	M326	0.1M HCl	-0.00142	Dull from brown stains no pits observed
8/27/2020	M326	0.1M HCl	-0.00091	Rainbow coloration, hints of shallow pits
7/30/2020	316L	0.1 M HCl	-0.00004	No clear change
8/5/2020	304L	0.1 M HCl	-0.00194	Mostly shiny, long shallow pits
8/27/2020	304B4	0.1M HCl	-0.00153	Dull, widespread deep pits
9/10/2020	304B5	0.1M HCl	-0.00336	Dull, widespread localized small pits

3.2 Acquisition of neutron absorbing materials

3.2.1 Borated stainless steels

The powder metallurgy, Grade A, corrosion samples are available at the INL [11]. These materials were developed by the Carpenter Technology Corporation (CarTech) to improve the borated alloy microstructure (boride shape and distribution) that will improve the alloys mechanical properties and corrosion resistance [12-14]. A reference of interest concludes that the corrosion resistance of a Grade A material (1.75% B) is equivalent to a Grade B material (1.1% B) in 15,000 ppm boric acid with 10 ppm Cl^- at 150 °C [14]. There were numerous inquiries and requests for Grade A test material made to the CarTech Research and Marketing groups with no success.

The development of BSS ingot metallurgy alloys was started in the 1970's [15]. These ingot metallurgy products were produced and marketed domestically by CarTech but their emphasis now is on the Grade A, powder metallurgy products.

For Grade B materials there are two commercial sources for these materials, Bohler Bleche GmbH & Co KG and Industeel USA LLC (Arcelor Mittal Group). Bohler Bleche (BB) has been in the business of producing these alloys for over thirty years. The BB Neutronit alloy and the major projects it has supported is described in a presentation to the Nuclear Regulatory Commission [16]. Discussions between the INL and BB resulted in BB furnishing two sample pieces to INL described in Table 5-6 [17].

These heats have a relatively high boron loading (1.25% and 1.27%) which would adversely affect the corrosion performance. These materials were not tested in the FY2020 program. Industeel is a wholly owned subsidiary of the ArcelorMittal Group who is the world's largest steel production company and has steel production facilities all over the world. Industeel, USA, handles their products in U.S. market. Their product designation is NUCL 304B4 [18]. The Industeel research center for advanced alloys (specialty plates, stainless and alloys) is located in Le Creusot, France. Both companies have recently produced BSS plate for large projects such as the International Thermonuclear Experimental Reactor (Tokamak) fusion project in Southern France.

Table 5. FA 2340348, heat E10729, 610 X 305 X 10 mm.

C	Si	Mn	P	S	Cr	Ni	N	Co	B
0.017	0.30	0.67	0.019	<0.0003	18.49	12.59	0.03	<0.05	1.27

Table 6. FA 2340722, Heat E10523, 610 X 305 X 5 mm.

C	Si	Mn	P	S	Cr	Ni	N	Co	B
0.021	0.28	0.62	0.017	<0.0003	18.40	12.54	0.03	<0.05	1.25

Reduced boron content alloy: A lowered boron content Grade B BSS employing enriched boron in an ingot metallurgy product might be suitable for service [1,19]. The basic concept was to use an addition of enriched boron (50% enrichment at a boron level of 0.5 wt.%) instead of the nominal natural boron level of approximately 1.25 wt.% to enhance corrosion resistance and mechanical properties through of the ingot metallurgy microstructure. BB and Industeel were approached to see if a small, lab scale heat with a boron level (natural) at 0.5% could be produced. Neither company expressed an interest.

3.2.2 Gd+B stainless steels

Powder metallurgy stainless steels with boron and gadolinium additions (SS+Gd+B): Another powder metallurgy product that is listed by CarTech is CARTECH Micro-Melt DuoSorb 316NU Alloy [20-22]. This material is not covered in an ASTM specification. It was apparently produced in limited quantities. The technical staff at CarTech are presently hoping to locate samples for this program.

Duplex and super duplex stainless steels with boron and/or gadolinium additions: Duplex (17-22% Cr) and super duplex ((25-27 wt.% Cr) are SSs with a nominal microstructure of 50% austenite and 50% ferrite phases. They have had extensive use in some seawater applications [23]. Two recent papers discuss the preparation and corrosion performance of duplex SSs with additions of boron and or gadolinium additions [24-25]. We requested any available sample materials from the author, but no reply was received. The material for these tests was produced under laboratory conditions.

3.2.3 Aluminum composites (Boral)

Boral (an aluminum cermet) was replaced in 2016 by the 3M Advanced Metal Matrix Composite. The material was dropped from the corrosion test program because this material was not designed for corrosion resistance in seawater.

3.2.4 Neutron absorbing corrosion resistant coatings

ANA coatings: A proposed use of a thermal spray coating is to provide enhanced neutron absorption and corrosion resistance performance to the surfaces of the chevron insert absorber plates [26]. Some of the neutron absorbing/corrosion resistant materials of construction being considered for this plate are BSS (ingot or powder metallurgy fabrication process) and ANA which are described in the corrosion test plan [1]. Some of the test conditions such as synthetic seawater at 30 ºC, 60 ºC, and 90 ºC are aggressive and could cause high rates of general and localized corrosion (pitting/crevice).

The nominal chevron insert thickness is 3 mm. Assuming that the fabrication process for this component is to cold bend a 3 mm strip product to shape, the ductility of the material must be evaluated. The addition

of Gd or B to a corrosion resistant alloy will decrease ductility with increasing addition levels. If the amount of B or Gd would need to be reduced in the chosen chevron alloy, a corrosion resistant/neutron absorbing coating might make up the difference.

The INL is in the process of receiving approximately 200 pounds of a thermal spray powder that has a base composition of Alloy C-22 (UNS NO6022, Ni-Cr-Mo chemistry)) with a 2 wt.% addition of Gadolinium. This material is similar in chemistry to the M327 heat in Table 1. The material is being procured through Haynes International, Kokomo, IN. The material will be applied to a 304L substrate by SNL using the cold spray process. The pieces will then be turned into corrosion samples.

Structurally amorphous materials (SAM): SAM2X5 (15.2% B): Another material that can be considered for coating applications is SAM2X5. An extensive thermal spray process development and corrosion testing programs were conducted by Lawrence Livermore National Laboratory (LLNL) on corrosion resistant, thermal neutron absorbing, iron based amorphous alloys with some favorable results [27-29]. This material was initially developed by the NanoSteel Company, Inc. The rights were assigned to the Lincoln Electric Company and this material is now designated as SHS 7574 HVOF.

3.2.5 NAM general observations

With the shutdown of the YMP, the demand for highly corrosion resistant, neutron absorbing materials is essentially non-existent. The ANA development program stopped with the closure of the NSNFP. As regards the lab scale production of ANA test material, there are concerns of possible vendors such as Haynes International on contamination of their development lab melt facility with gadolinium. Another factor is the effect of the pandemic on the reduced sale of high temperature, aero-space alloys by possible ANA producers such as Haynes, International and Special Metals, Corp which could affect the development of alloy based on the YMP experience. The ingot metallurgy BSSs are available from two European mills. An ANA powder product for thermal spray is available from Haynes International. CarTech is not in production of their powder metallurgy, borated and boron/gadolinium alloys. To obtain these alloys, a quotation request from the INL could be sent through procurement channels to gauge interest. SAM2X5 powder is currently available from Lincoln Electric as SHS 7574 HVOF. Technology for producing coatings and bulk materials has advanced in the past decade, providing opportunities to produce unique materials including grading the composition to optimize corrosion performance for exposed surfaces.

4. Initial conclusions

Experiments for the initial testing campaign have been completed with post-test specimen analysis and finalized assessments to be completed. Without a complete information set, an extensive discussion will not be presented. The results for the NAM materials appear to follow what was previously observed in testing. Based on the CPP results, all three environments present marginal stability for the NAM materials. Alloy 22 was the only material that was clearly suitable for all three environments. The ANA materials need further assessment, perhaps considering some of the specific aspects of the reactive secondary phase. The performance of 304B specimens did not appear significantly different than 304L initial examination. There was a significant drop-off in performance noted between 304B6 (1.50–1.74% B) and 304B5 (1.25–1.49% B) [11] in previous work in this lab [9]. Note that the three alloys tested the following B concentrations for 304B4, 304B5 and 304B6 are 1.17, 1.32 and 1.67 wt.% respectively. The gap between 304B5 and 304B6 is significantly higher. The use of austenitic steel to normalize performance was very useful, which previous work did not examine. This report will be updated and expanded to incorporate more results, analysis, and discussion.

5. Testing activities for FY21

In addition to completing the 2020 corrosion testing campaign, future activities are planned to broaden the material palette to include specimens produced by advanced manufacturing practices. These will include both alloys and coatings. Coated specimens will be tested using a slightly different cell designed to seal to one side of a flat specimen. While a search for new BSS materials has not been fruitful, search for materials containing boron will continue.

5.1 New alloy testing

- ORNL “3D printed” specimen corrosion testing.
- Duplex and super duplex SSs have a long history of use in components for seawater service. Research papers discussed earlier show that B and Gd can be added to these alloys [24-25]. A literature review should be conducted to see how these alloys (without B or Gd addition) might be suitable for our test conditions.

5.2 NAM coatings

- A NAM thermal spray coating consisting of boron carbide powder co-spayed with Alloy C22 powder.
- SNL is developing coating parameters and will fabricate corrosion coupons using an ANA powder (Hastelloy C-22 with 2 wt.% Gd). These coupons should be added to the corrosion test program.

- For a comparison purposes, corrosion coupons should be prepared with Alloy C-22 powder (same process and parameters as used for the ANA powder application) and tested for baseline data comparison purposes. (SNL)
- SAM2X5 coating testing. Subject matter experts in the thermal spray process (powder feedstock application) should evaluate the proper process for application of this material to corrosion coupons/chevron inserts. The LLNL program used both high velocity oxygen fuel (HVOF) and high velocity air fuel (HVAF). Based on the findings, obtain SAM2X5 powder and have corrosion coupons prepared with the recommended process. These coupons should be included in the 2021 corrosion test program.

5.3. Follow-on corrosion testing to support FY20 testing

- ANA surface condition corrosion testing. Corrosion testing with the ANA material shows that the dissolution of the gadolinide (Ni_5Gd) phases that intersect the surface results in a higher initial corrosion current that slowly fades away over time. A useful data set would be to remove this phase with a "pickling solution" that the alloy mills use to remove surface oxides after hot rolling. This may give a more representative corrosion rate in a shorter test period.
- Perform any additional tests to clear up remaining questions from FY20 testing.

References

1) INL PLN 6095, *Neutron Absorber Material Test Plan*, INL/EXT-20-58534, 2020.

2) ASTM G5 -14 (2014) *Standard Reference Test Method for Making Potentiodynamic Anodic Polarization Measurements*, ASTM International, West Conshohocken, PA.

3) ASTM D1141 – 99 (2013) *Standard Practice for the Preparation of Substitute Ocean Water*, ASTM International, West Conshohocken, PA.

4) ASTM G59 − 97 (Reapproved 2014), *Conducting Potentiodynamic Polarization Resistance Measurements*, ASTM International, West Conshohocken, PA.

5) ASTM G102 – 89 (2015) *Standard Practice for Calculation of Corrosion Rates and Related Information from Electrochemical Measurements*, ASTM International, West Conshohocken, PA.

6) R.C. Pistorius, *The Effect of Some Fundamental Aspects of the Pitting Corrosion of Stainless Steel on Electrochemical Noise Measurements*, Electrochemical Noise Measurement for Corrosion Applications, ASTM STP 1277, American Society for Testing and Materials, 1996, pp. 343-358.

7) R. M. Kain, *Crevice Corrosion Behavior of Stainless Steel in Seawater and Related Environments*, Corrosion **40** (1984) 313.

8) R. E. Mizia and T. E. Lister, *Accelerated Testing of Neutron-Absorbing Alloys for Nuclear Criticality Control*, Nuclear Technology **176** (2011) 9.

9) T.E. Lister, R.E. Mizia, A.W. Erickson, B.S. Matteson, *General and Localized Corrosion of Borated Stainless Steels*, NACE Corrosion 2008, Paper 08590, New Orleans, LA.

10) R.B. Rebak, Factors Affecting the Crevice Corrosion Susceptibility of Alloy 22, NACE Corrosion 2005, Paper 05610, Houston, TX.

11) ASTM A 887-89 (2014) *Standard Specification for Borated Stainless Steel Plate, Sheet, and Strip for Nuclear Application*, ASTM International, West Conshohocken, PA.

12) J.W. Martin, *Effects of Processing and Microstructure on the Mechanical Properties of Boron-Containing Austenitic Stainless Steels,* Proceedings of the Symposium on Waste Management, University of Arizona, Tucson, AZ. 1989.

13) Carpenter Technology Corporation Datasheet, *CarTech Micro-Melt NeutroSorb Plus Alloys,* Date 03/04/09.

14) R.S. Brown, (CarTech), *Corrosion Resistance of Borated Stainless Steels Carpenter Neutrosorb Plus (Grade A) and Neutrosorb (Grade B)*, CarTech Internal Research Reports, 03/28/91

15) H.J. Goldschmidt, Effect of boron in 18% Cr, 25% Ni austenitic steel, The Journal of the Iron and Steel Institute, Nov., 1971.

16) A. Presti, *Shielding Materials for Nuclear Industry*, NRC Meeting – NAMs, March 14, 2013.

17) Email, Jeremy Steinman (Bohler Bleche) to Ronald Mizia (SNF Project), March 30, 2020.

18) Industeel/Arcelor Mittal NUCL 304B4, dated 12/2019.

19) H. Ha, J.H. Jang, T. Lee, C. Won, C. Lee, J. Moon 1 and C. Lee, *Investigation of the Localized Corrosion and Passive Behavior of Type 304 Stainless Steels with 0.2–1.8 wt % B*, Materials 2018, 11.

20) Carpenter Technology Corporation Datasheet, *CarTech Micro-Melt DuoSorb 316NU Alloys, Edition D Date 1/20/2016.*

21) M.L. Schmidt, G.J. Del Corso, K.A. Klankowski, L.W. Lherbier, and D.J. Novotnak, *Review of the Development and Testing of a New Family of Boron and Gadolinium-Bearing Dual Thermal Neutron Absorbing Alloys*, Waste Management 2013 Conference, Feb. 24 – 28, 2013.

22) United States Patent, Patent Number: US9,267,192 B2, Michael L. Schmidt, Gregory J. Del Corso, Patrick C. Ray, Ning Ma, *Processable High Thermal Neutron Absorbing Fe-Base Alloy Powder,* Feb. 23, 2016.

23) B. Wallen, *Corrosion of Duplex Stainless Steels in Seawater,* Duplex Stainless Steels 97: 5th World Conference [organized by: Stainless Steel World. Fifth World Conference on Duplex Stainless Steels, Maastricht, the Netherlands, 21-23 October 1997].

24) Y. Choi, B.M. Moon, D.S. Song, *Fabrication of Gd Containing Duplex Stainless Steel Sheet for Neutron Absorbing Structural Materials,* Nuclear Engineering and Technology **45** (2013) 689-694.

25) M. Jung, Y. Baik, Y. Choi, and D.S. Sohn, *Corrosion and Mechanical Properties of Hot-Rolled 0.5%Gd-0.8%B Stainless Steels in a Simulated Nuclear Waste Treatment Solution*, Nuclear Engineering and Technology **51** (2019) 207-213.

26) Options for Future Fuel/Basket Modifications for DPC Disposition, Section 2.2, Sandia National Laboratories, Albuquerque, NM, M4SF-20SN010305051, Rev. 1, June 2020.

27) P.D. Hailey, J.C., Farmer, S.D. Day, R.B. Rebak, *Anodic Behavior of SAM2X5 Material Applied as Amorphous Coatings,* Materials Science and Technology, (MS&T) 2007.

28) J.C. Farmer, et al, *Corrosion Resistance of Amorphous $Fe_{49.7}Cr_{17.7}Mn_{1.9}Mo_{7.4}W_{1.6}B_{15.2}C_{3.8}Si_{2.4}$ Coating: A New Criticality Control Material*, Nuclear Technology **161** (2008) 169-189, DOI:10.13182/NT08-A3921.

29) J. Blink, J. Farmer, J. Choi, and S. Saw, *Applications in the Nuclear Industry for Thermal Spray Amorphous Metal and Ceramic Coatings*, Metallurgical and Materials Transactions A, 1344-Volume 40A, June 2009.